STRUCTURAL BIOLOGY COMMUNICATIONS

ISSN 2053-230X

Neutron and X-ray analysis of the Fenna–Matthews–Olson photosynthetic antenna complex from *Prosthecochloris aestuarii*

Xun Lu,[a] Brinda Selvaraj,[a] Sudipa Ghimire-Rijal,[a] Gregory S. Orf,[b]‡ Flora Meilleur,[a,c] Robert E. Blankenship,[b] Matthew J. Cuneo[a,d] and Dean A. A. Myles[a]*

[a]Neutron Science Directorate, Oak Ridge National Laboratory, Oak Ridge, TN 37831, USA, [b]Departments of Biology and Chemistry, Washington University in St Louis, St Louis, MO 63130, USA, [c]Department of Molecular and Structural Biochemistry, North Carolina State University, Campus Box 7622, Raleigh, NC 27695, USA, and [d]Department of Structural Biology, St Jude Children's Research Hospital, Memphis, TN 38105, USA. *Correspondence e-mail: mylesda@ornl.gov

Received 18 September 2018
Accepted 16 January 2019

Edited by M. W. Bowler, European Molecular Biology Laboratory, France

‡ Present address: Center for Bioenergy and Photosynthesis, School of Molecular Sciences, Arizona State University, Tempe, AZ 85287, USA.

Keywords: neutron crystallography; photosynthesis; hydrogen; site energy; neutron diffraction; Fenna–Matthews–Olson protein; *Prosthecochloris aestuarii*.

PDB reference: Fenna–Matthews–Olson antenna complex, 6mez

Supporting information: this article has supporting information at journals.iucr.org/f

The Fenna–Matthews–Olson protein from *Prosthecochloris aestuarii* (*Pa*FMO) has been crystallized in a new form that is amenable to high-resolution X-ray and neutron analysis. The crystals belonged to space group $H3$, with unit-cell parameters $a = b = 83.64$, $c = 294.78$ Å, and diffracted X-rays to ∼1.7 Å resolution at room temperature. Large *Pa*FMO crystals grown to volumes of 0.3–0.5 mm^3 diffracted neutrons to 2.2 Å resolution on the MaNDi neutron diffractometer at the Spallation Neutron Source. The resolution of the neutron data will allow direct determination of the positions of H atoms in the structure, which are believed to be fundamentally important in tuning the individual excitation energies of bacteriochlorophylls in this archetypal photosynthetic antenna complex. This is one of the largest unit-cell systems yet studied using neutron diffraction, and will allow the first high-resolution neutron analysis of a photosynthetic antenna complex.

1. Introduction

Photosynthetic antenna complexes capture photonic energy from the sun and transfer the excitation energy to the photosynthetic reaction center, driving the photochemical reactions that support most life on Earth. These complexes function by incorporating sets of specialized pigments within a protein scaffold that modulates and tunes their spectral response and energy-transfer properties. In green sulfur bacteria, the Fenna–Matthews–Olson (FMO) protein functions as a 'wire' that mediates energy transfer between the light-harvesting chlorosomes and the reaction center (Fig. 1; Orf & Blankenship, 2013; Blankenship, 2014). The FMO complex exists as a homotrimer, with each monomer containing seven bacteriochlorophyll (BChl) pigments embedded in a large, rigid open-face β-sandwich domain (Matthews *et al.*, 1979). An eighth BChl is located at the interface between the subunits in the trimer (Tronrud *et al.*, 2009). The precise organization and assembly of BChls within the array and their interactions with the surrounding protein scaffold exquisitely tune and control the energy levels of the individual pigment excitonic states, creating an energy funnel that guides the flow of energy down through the protein to the reaction center (Müh *et al.*, 2007; Schmidt am Busch *et al.*, 2011). While the electronic energy-transfer process in FMO has been extensively studied and is broadly understood, debate remains on the precise details of the molecular mechanisms and pathways

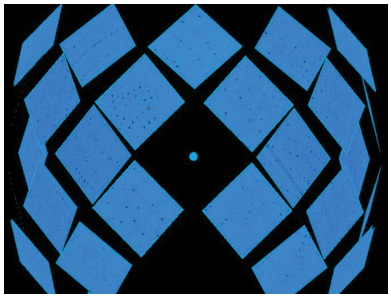

Table 1
Crystallization.

Method	Vapor diffusion
Plate type	Sitting drop
Temperature (K)	293
Protein concentration (mg ml^{-1})	12
Buffer composition of protein solution	20 m*M* Tris, 40 m*M* NaCl pH 8.0
Composition of reservoir solution	22.5% saturated ammonium sulfate, 0.1 *M* sodium acetate pH 5.0
Volume and ratio of drop	1100 µl (1:1)
Volume of reservoir (ml)	50

involved (Engel *et al.*, 2007; Panitchayangkoon *et al.*, 2010; Duan *et al.*, 2017).

The X-ray structures of FMO proteins from several strains (Camara-Artigas *et al.*, 2003; Ben-Shem *et al.*, 2004; Larson *et al.*, 2011) and recent mutants (Saer *et al.*, 2016; Orf *et al.*, 2016) show strong similarities in overall protein–pigment architectures, but the proteins exhibit differences in characteristic spectral properties that are not fully understood in terms of the available structural models. Each BChl experiences a different chemical environment within the monomer, through which interactions with the neighboring protein residues and solvent molecules distort the conformation and planarity of the tetrapyrrole ring, imparting each BChl with its own particular site energy. The local charge distribution and the hydrogen-bonding interactions with the surrounding protein and solvent are therefore thought to be important in tuning the excitation energy-transfer pathway. Although the FMO complex has been extensively characterized by X-ray crystallography, computer simulations and spectroscopic analysis, explicit information on how H atoms and water molecules may contribute to the fine-tuning of the pigment excitation energy has been lacking or inferred. Neutron diffraction is uniquely sensitive to the location of H atoms in biological structures (for a review, see O'Dell *et al.*, 2016). Therefore, in order to better understand how individual BChl site energies are modulated by local pigment–solvent–protein interactions, we have produced a new crystal form of the FMO protein from *Prosthecochloris aestuarii* (*Pa*FMO) that diffracted neutrons to a resolution of 2.2 Å at the Spallation Neutron Source (SNS) at Oak Ridge National Laboratory (ORNL). Here, we report the preparation, crystallization and preliminary X-ray and neutron analysis of this archetypal photosynthetic antenna complex.

2. Materials and methods

2.1. Macromolecule production

The *Pa*FMO protein was purified from *P. aestuarii* cell cultures following established protocols (Orf *et al.*, 2014). Briefly, the cells were disrupted by sonication, centrifuged at low speed to remove debris and centrifuged again at 186 500*g* for 2 h in a buffer consisting of 20 m*M* Tris pH 8.0. The membrane-containing pellet was resuspended in the same buffer after centrifugation, and sodium carbonate was added through dialysis to a final concentration of 0.4 *M* over at least 24 h. The solution was then centrifuged at 307 500*g* for 2 h, after which the supernatant was collected and extensively dialyzed into 20 m*M* Tris pH 8.0. The dialyzed material was loaded onto Q Sepharose resin (GE) and elution was carried out with an NaCl gradient, with *Pa*FMO typically eluting at NaCl concentrations of >300 m*M*. Fractions containing *Pa*FMO were pooled and concentrated before loading them onto a Superdex S75 gel-filtration column (GE) equilibrated with 20 m*M* Tris, 40 m*M* NaCl pH 8.0. The peak from the gel-filtration column was collected and concentrated before final purification on a HiTrap Q column (GE). The purified *Pa*FMO protein was then concentrated to 12 mg ml^{-1} for crystallographic studies.

2.2. Crystallization

FMO crystals were grown in mother liquor consisting of 25% ammonium sulfate, 0.1 *M* sodium acetate pH 5.0 at 22°C by the sitting-drop vapor-diffusion method (Table 1). The crystals belonged to the trigonal space group *H*3, with unit-cell parameters $a = b = 83.64$, $c = 294.78$ Å. Crystals suitable for neutron diffraction analysis were grown by the sitting-drop vapor-diffusion method in a grease-sealed nine-well sandwich box with 50 ml reservoir solution. 50–1100 µl of protein solution was mixed with the same volume of reservoir solution consisting of 22.5% saturated ammonium sulfate, 0.1 *M* sodium acetate pH 5.0. All solutions were filtered through 0.2 µm Millipore filters. As the growth conditions were refined, the diffraction quality was assessed using the IMAGINE macromolecular neutron diffractometer at the ORNL High Flux Isotope Reactor neutron source (Meilleur *et al.*, 2013; Schröder *et al.*, 2018). IMAGINE uses a broad-bandpass Laue configuration (2.8 to ∼20 Å) to enable rapid (15 min exposure per frame) crystal screening (Fig. 2).

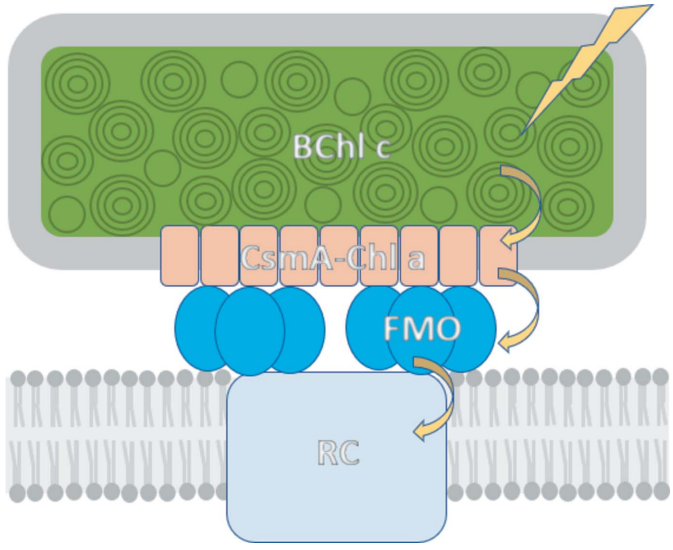

Figure 1
Model of the energy-transfer pathway in the photosynthetic system of *P. aestuarii*. Arrows show sequential energy transfer from light capture by BChl *c* arrays in the chlorosome, down through the CsmA protein in the baseplate and the trimeric Fenna–Matthew–Olson (FMO) complex to the photosynthetic reaction center (RC).

Ultimately, large single crystals (with a size of about 0.3 mm^3) could be reproducibly grown over two months.

2.3. Data collection and processing

Room-temperature X-ray data extending to 1.7 Å resolution were collected using a Rigaku MicroMax-007 HF rotating-anode X-ray generator at ORNL. The data were processed and scaled in *HKL*-3000 (Minor *et al.*, 2006). Data-collection statistics are given in Table 2.

To reduce the incoherent neutron scattering background from hydrogen, exchangeable hydrogen in the crystal was replaced by deuterium through vapor-exchange equilibration against a D_2O reservoir solution containing 25% saturated ammonium sulfate and 0.1 *M* sodium acetate (pD 5.0). Crystals were equilibrated for one month prior to neutron data collection, during which the reservoir solution was changed three times. A single *Pa*FMO crystal of ∼0.3 mm^3 in volume was mounted in a 0.8 mm diameter quartz capillary with a plug of deuterated exchange solution and sealed with wax for neutron data collection. The neutron quasi-Laue data set was collected at room temperature using the MaNDi macromolecular neutron crystallography instrument at the SNS. MaNDi is specifically designed for the analysis of large-unit-cell (>150 Å) systems (Schultz *et al.*, 2005; Coates *et al.*, 2015). Time-of-flight (TOF) neutron diffraction data were recorded to 2.2 Å resolution using neutrons between 2.0 and 4.0 Å wavelength. The ω angle was fixed at 90° for data collection. Nine images were collected with 48 h exposures per frame and with the crystal rotated by 10° in φ between images. A representative quasi-Laue neutron diffraction pattern from MaNDi is shown in Fig. 3. The data were processed and integrated using the *Mantid* package (Arnold *et al.*, 2014) and were wavelength-normalized using *LAUENORM* from the *LAUEGEN* package (Campbell *et al.*, 1998). *LAUENORM* performs a wavelength normalization of the Laue data and scaling between Laue diffraction images. Data-reduction statistics are shown in Table 2.

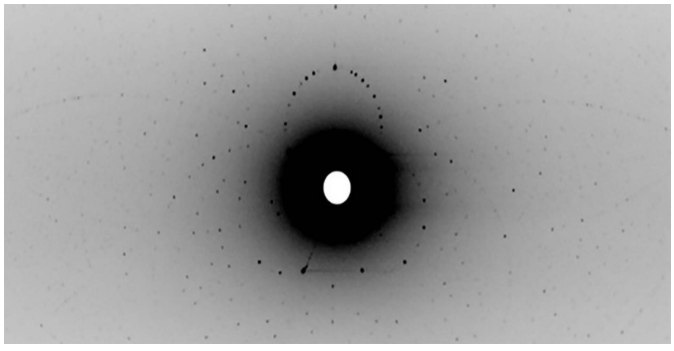

Figure 2
A Laue neutron diffraction image recorded from a $^1H/^2H$ vapor-exchanged FMO crystal on the CG-4D IMAGINE beamline at the High Flux Isotope Reactor (HFIR), Oak Ridge National Laboratory.

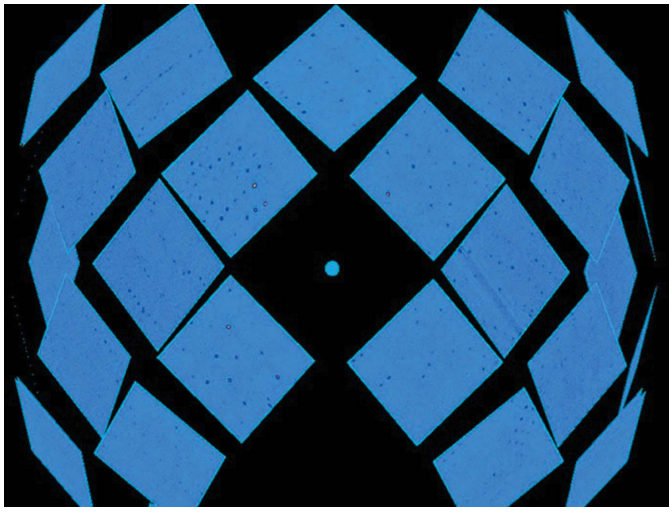

Figure 3
The diffraction pattern of *Pa*FMO from the spherical detector array of the MaNDi instrument at the Spallation Neutron Source, Oak Ridge National Laboratory.

Table 2
X-ray and neutron data collection and processing.

Values in parentheses are for the outer shell.

	Neutron	X-ray
Diffraction source	MaNDi, ORNL	Rigaku MicroMax-007 HF rotating-anode generator, ORNL
Wavelength (Å)	2–4	1.5417
Temperature (K)	293	293
Detector	32 Anger cameras	R-AXIS IV
Crystal-to-detector distance (mm)	420–450	120
Rotation range per image (°)	0†	0.25
Total rotation range (°)	90	132
Exposure time per image (s)	48 h	30 s
Space group	*H*3	*H*3
a, *b*, *c*‡ (Å)	83.16, 83.16, 294.32	83.64, 83.64, 294.78
Resolution range (Å)	14.63–2.20 (2.28–2.20)	19.65–1.74
Total No. of reflections	29653	73470
No. of unique reflections	2344	3850
Completeness (%)	76.1 (60.3)	93.3 (49.2)
Multiplicity	2.5 (1.6)	3.6 (3.3)
$\langle I/\sigma(I)\rangle$	5.7 (2.1)	10.8 (2.4)
R_{merge}	0.173 (0.223)	0.061 (0.409)
Overall *B* factor from Wilson plot ($Å^2$)		18.2

† Still quasi-Laue diffraction images were collected at 10° steps in φ rotation at three unique crystal orientations and were combined into a single data set. ‡ The absolute unit-cell parameters determined from X-ray monochromatic data were used in refinement. The axial ratios from Laue refinement scale to the absolute cell.

2.4. Structure solution and refinement

The X-ray structure was solved by molecular replacement in *Phaser* (McCoy *et al.*, 2007) with PDB entry 3eoj (Tronrud *et al.*, 2009) as the starting model; the model was built in *Coot* (Emsley *et al.*, 2010) and refined in *PHENIX* (Adams *et al.*, 2010). Details of the X-ray structure and refinement are shown in Table 3.

3. Results and discussion

*Pa*FMO was purified from cell cultures of *P. aestuarii*, yielding 80 mg protein from 30 g of wet cell paste. Initial efforts to

Table 3
X-ray structure and refinement.

Values in parentheses are for the outer shell.

Resolution range (Å)	19.65–1.74 (1.804–1.740)
Completeness (%)	93.4 (49.16)
σ Cutoff	10.8 (2.4)
No. of reflections, working set	73453 (3850)
No. of reflections, test set	3693 (194)
Final R_{cryst}	0.1341 (0.1913)
Final R_{free}	0.1584 (0.2416)
Cruickshank DPI	0.126
No. of non-H atoms	
Protein	6320
Ligand	1018
Water	474
Total	7812
R.m.s. deviations	
Bonds (Å)	0.011
Angles (°)	1.30
Average B factors (Å^2)	
Overall	22.03
Protein	21.26
Ligand	20.20
Water	36.29
Ramachandran plot	
Favored regions (%)	98.79
Additionally allowed (%)	1.21
Outliers (%)	0

grow large crystals (>0.1 mm^3) of the published $P6_3$ crystal form of *Pa*FMO (PDB entry 3eoj), which diffract X-rays to high resolution (1.3 Å), were unsuccessful. New crystallization conditions were obtained that produced a new *H*3 crystal form with unit-cell parameters $a = b = 83.64$, $c = 294.78$ Å. The structure was solved at 1.7 Å resolution by molecular replacement using PDB entry 3eoj. This new crystal form has two FMO monomers in the asymmetric unit (PDB entry 6mez). Each FMO monomer contains seven BChl molecules that are held in precise orientation by the protein scaffold within a rigid 'taco-shell' core formed from two antiparallel β-sheets. As expected, the room-temperature structure is closely similar to the structure in PDB entry 3eoj, with a root-mean-square deviation (r.m.s.d.) of 0.240 Å for 294 C^α atoms. However, density for the eighth BChl, which is found at various occupancies in the interface between adjacent monomers in other FMO proteins (Li *et al.*, 1997; Camara-Artigas *et al.*, 2003, Ben-Shem *et al.*, 2004; Larson *et al.*, 2011), and which is modeled in two conformations in PDB entry 3eoj (Tronrud *et al.*, 2009), was not resolved in this 1.7 Å resolution structure. We note that the eighth BChl molecule is susceptible to depletion or loss during purification of the *Pa*FMO complex, and has been reported as lost or variably occupied in other spectroscopic and structural studies (Tronrud *et al.*, 2009)

After extensive trials, large crystals suitable for neutron diffraction were grown from a protein concentration of 12 mg ml^{-1} and sitting-drop volumes of up to 2000 µl (Fig. 1). The crystals grew to a volume of about 0.3–0.5 mm^3 after a month. Crystals selected for neutron diffraction were equilibrated against a deuterated reservoir solution to exchange labile H atoms with deuterium and reduce the incoherent neutron diffraction background. Ultimately, a crystal with a volume of 0.3 mm^3 was selected for room-temperature neutron data collection, producing data to 2.2 Å resolution. The final data set has 29 653 reflections, which reduced to 2344 unique reflections with an R_{merge} of 17.3%. Full processing statistics for the neutron data are reported in Table 2. We note that the R_{merge} statistics are comparable to those reported for other neutron Laue experiments (Meilleur *et al.*, 2013; Coates *et al.*, 2015). The available neutron beam time (18 days) and the relatively weak diffraction from this large-unit-cell system resulted in a final data set that was 77% complete to 2.2 Å resolution, beyond which the data quality and completeness deteriorate. This study is especially notable in representing one of the largest unit-cell edge (294 Å), largest unit-cell volume ($V = 1.7 \times 10^7$ Å^3) and smallest crystal volume/unit cell systems yet studied using neutrons, marking a new threshold for spallation neutron protein crystallography.

Although extensively studied, the available X-ray structures of FMO lack sufficient resolution to visualize individual H atoms, and questions remain concerning the protonation states of key protein residues and how the individual site energies of each BChl may be modulated by hydrogen-bonding interactions with the protein–solvent environment. The neutron structure of *Pa*FMO (the first neutron structure of a photosynthetic complex) will aid in directly visualizing these interactions. The initial nuclear density for the backbone amides and solvent molecules indicates extensive hydrogen-bonded protein–pigment–solvent networks. Refinement of the structure using both neutron and high-resolution X-ray data is ongoing. Thus, a fully refined structure of FMO may yield detailed insights into the specific local environment around each BChl and help to understand how the protein–pigment–solvent interactions contribute to the efficient energy-transfer dynamics.

Acknowledgements

This research used resources at the High Flux Isotope Reactor and the Spallation Neutron Source, which are DOE Office of Science User Facilities operated by Oak Ridge National Laboratory.

Funding information

This work was supported by the Photosynthetic Antenna Research Center, an Energy Frontier Research Center funded by the US Department of Energy, Office of Science, Office of Basic Energy Sciences under Award DE-SC 0001035 (REB, DAAM).

References

Adams, P. D., Afonine, P. V., Bunkóczi, G., Chen, V. B., Davis, I. W., Echols, N., Headd, J. J., Hung, L.-W., Kapral, G. J., Grosse-Kunstleve, R. W., McCoy, A. J., Moriarty, N. W., Oeffner, R., Read, R. J., Richardson, D. C., Richardson, J. S., Terwilliger, T. C. & Zwart, P. H. (2010). *Acta Cryst.* D**66**, 213–221.

Arnold, O., Bilheux, J. C., Borreguero, J. M., Buts, A., Campbell, S. I., Chapon, L., Doucet, M., Draper, N., Ferraz Leal, R., Gigg, M. A., Lynch, V. E., Markvardsen, A., Mikkelson, D. J., Mikkelson, R. L., Miller, R., Palmen, K., Parker, P., Passos, G., Perring, T. G., Peterson, P. F., Ren, S., Reuter, M. A., Savici, A. T., Taylor, J. W.,

Taylor, R. J., Tolchenov, R., Zhou, W. & Zikovsky, J. (2014). *Nucl. Instrum. Methods Phys. Res. A*, **764**, 156–166.
Ben-Shem, A., Frolow, F. & Nelson, N. (2004). *FEBS Lett.* **564**, 274–280.
Blankenship, R. E. (2014). *Molecular Mechanisms of Photosynthesis*, 2nd ed. Chichester: John Wiley & Sons.
Camara-Artigas, A., Blankenship, R. E. & Allen, J. P. (2003). *Photosynth. Res.* **75**, 49–55.
Campbell, J. W., Hao, Q., Harding, M. M., Nguti, N. D. & Wilkinson, C. (1998). *J. Appl. Cryst.* **31**, 496–502.
Coates, L., Cuneo, M. J., Frost, M. J., He, J., Weiss, K. L., Tomanicek, S. J., McFeeters, H., Vandavasi, V. G., Langan, P. & Iverson, E. B. (2015). *J. Appl. Cryst.* **48**, 1302–1306.
Duan, H.-G., Prokhorenko, V. I., Cogdell, R. J., Ashraf, K., Stevens, A. L., Thorwart, M. & Miller, R. J. D. (2017). *Proc. Natl Acad. Sci. USA*, **114**, 8493–8498.
Emsley, P., Lohkamp, B., Scott, W. G. & Cowtan, K. (2010). *Acta Cryst.* D**66**, 486–501.
Engel, G. S., Calhoun, T. R., Read, E. L., Ahn, T.-K., Mancal, T., Cheng, Y.-C., Blankenship, R. E. & Fleming, G. R. (2007). *Nature (London)*, **446**, 782–786.
Larson, C. R., Seng, C. O., Lauman, L., Matthies, H. J., Wen, J., Blankenship, R. E. & Allen, J. P. (2011). *Photosynth. Res.* **107**, 139–150.
Li, Y.-F., Zhou, W., Blankenship, R. E. & Allen, J. P. (1997). *J. Mol. Biol.* **271**, 456–471.
Matthews, B. W., Fenna, R. E., Bolognesi, M. C., Schmid, M. F. & Olson, J. M. (1979). *J. Mol. Biol.* **131**, 259–285.
McCoy, A. J., Grosse-Kunstleve, R. W., Adams, P. D., Winn, M. D., Storoni, L. C. & Read, R. J. (2007). *J. Appl. Cryst.* **40**, 658–674.
Meilleur, F., Munshi, P., Robertson, L., Stoica, A. D., Crow, L., Kovalevsky, A., Koritsanszky, T., Chakoumakos, B. C., Blessing, R. & Myles, D. A. A. (2013). *Acta Cryst.* D**69**, 2157–2160.
Minor, W., Cymborowski, M., Otwinowski, Z. & Chruszcz, M. (2006). *Acta Cryst.* D**62**, 859–866.
Müh, F., Madjet, M. E., Adolphs, J., Abdurahman, A., Rabenstein, B., Ishikita, H., Knapp, E. W. & Renger, T. (2007). *Proc. Natl Acad. Sci. USA*, **104**, 16862–16867.
O'Dell, W. B., Bodenheimer, A. M. & Meilleur, F. (2016). *Arch. Biochem. Biophys.* **602**, 48–60.
Orf, G. S. & Blankenship, R. E. (2013). *Photosynth. Res.* **116**, 315–331.
Orf, G. S., Niedzwiedzki, D. M. & Blankenship, R. E. (2014). *J. Phys. Chem. B*, **118**, 2058–2069.
Orf, G. S., Saer, R. G., Niedzwiedzki, D. M., Zhang, H., McIntosh, C. L., Schultz, J. W., Mirica, L. M. & Blankenship, R. E. (2016). *Proc. Natl Acad. Sci. USA*, **113**, E4486–E4493.
Panitchayangkoon, G., Hayes, D., Fransted, K. A., Caram, J. R., Harel, E., Wen, J., Blankenship, R. E. & Engel, G. S. (2010). *Proc. Natl Acad. Sci. USA*, **107**, 12766–12770.
Saer, R., Orf, G. S., Lu, X., Zhang, H., Cuneo, M. J., Myles, D. A. A. & Blankenship, R. E. (2016). *Biochim. Biophys. Acta*, **1857**, 1455–1463.
Schmidt Am Busch, M., Müh, F., El-Amine Madjet, M. & Renger, T. (2011). *J. Phys. Chem. Lett.* **2**, 93–98.
Schröder, G. C., O'Dell, W. B., Myles, D. A. A., Kovalevsky, A. & Meilleur, F. (2018). *Acta Cryst.* D**74**, 778–786.
Schultz, A. J., Thiyagarajan, P., Hodges, J. P., Rehm, C., Myles, D. A. A., Langan, P. & Mesecar, A. D. (2005). *J. Appl. Cryst.* **38**, 964–974.
Tronrud, D. E., Wen, J., Gay, L. & Blankenship, R. E. (2009). *Photosynth. Res.* **100**, 79–87.